Incorporation of Mn into the vacant T-atom sites of a BEA zeolite as isolated, mononuclear Mn: FTIR, XPS, EPR and DR UV-Vis studies

R. Baran, L. Valentin, Stanislaw Dzwigaj

Incorporation of Mn into the Vacant T–Atom Sites of BEA Zeolite as Isolated, Mononuclear Mn: FTIR, XPS, EPR and DR UV−Vis Studies

Rafal Baran[1,2,3], Laetitia Valentin[2,3] and Stanislaw Dzwigaj[2,3,*]

[1]AGH University of Science and Technology al. A. Mickiewicza 30, 30-059 Krakow, Poland

[2]Sorbonne Universités, UPMC Univ Paris 06, UMR 7197, Laboratoire de Réactivité de Surface, F-75005, Paris, France

[3]CNRS, UMR 7197, Laboratoire de Réactivité de Surface, F-75005, Paris, France

Figures: 10

Tables: 4

Keywords: Manganese, Beta zeolite, mononuclear Mn, FTIR, EPR

*Corresponding author

Stanislaw Dzwigaj, e-mail : stanislaw.dzwigaj@upmc.fr, fax : +33 1 44 27 21 13

Abstract

A MnSiBEA zeolite has been prepared by a two-step postsynthesis procedure which consisted, in the first step, of a treatment of tetraethylammonium BEA zeolite by nitric acid with formation of vacant T-atom sites and then, in the second step, of an incorporation of Mn ions into framework of resulted SiBEA zeolite by their reaction with silanol group of vacant T-atom sites. The incorporation of Mn ions into the framework of SiBEA zeolite has been evidenced by XRD. The formation of isolated mononuclear Mn(II) and Mn(III) in MnSiBEA zeolite has been shown by FTIR, diffuse reflectance UV−vis, EPR and XPS. Acidic properties of mononuclear manganese species have been investigated by FTIR spectroscopy using pyridine as the probe molecule. The changes in the oxidation state of Mn species under various treatments have been proved by EPR.

1. Introduction

Increasing interesting in manganese-containing zeolite catalysts have been observed over several last years, especially in the processes important for environment protection such as selective catalytic reduction of NO with ammonia[1–3] and oxidation of volatile organic compounds (VOC)[4–6] because of their high efficiency. The most often methods used for the preparation of Mn-containing zeolites are conventional techniques of postsynthesis modification such as wet impregnation and ion-exchange[1,7,8] or direct synthesis in hydrothermal conditions.[9–11] However, manganese in Mn-containing zeolites obtained by these conventional preparation procedures may be present at various oxidation states and environment because these preparation methods do not allow controlling state of manganese in the zeolite structure. As a result Mn-containing zeolite materials with different form of manganese species e.g., isolated ions in framework and extra-framework positions, single oxides clusters (MnO, Mn_2O_3 and MnO_2) or mixed oxides such as Mn_3O_4 could be formed.

Presence of different form of active sites might lead to poor selectivity in many reactions but major requirement for the catalysts preparation is to obtain a stable and high selective catalyst to hinder side reactions and to avoid fast deactivation. Thus, the optimisations of current methods as well as development of new methods of zeolite catalyst preparation have been strongly demanded.

In this work we have used a two-step postsynthesis method developed earlier by Dzwigaj et al.[12–16] to obtain Mn-containing SiBEA zeolite with isolated, mononuclear Mn species. The incorporation of manganese ions into zeolite framework was evidenced by XRD, FTIR, diffuse reflectance UV−vis, XPS and EPR.

2. Experimental section

2.1. Materials

Two portions of the tetraethylammonium BEA (TEABEA) zeolite (Si/Al = 17) provided by RIPP (China) were prepared. The first one was used to obtain HAlBEA zeolite by the way described in in our earlier work.[17] The second fraction of TEABEA zeolite was dealuminated by a treatment with nitric acid solution of C = 13 mol L^{-1} at 353 K for 4 h, to obtain aluminum free SiBEA zeolite, and then it was washed several times with distilled water and dried at 368 K overnight. In the next step two portions of SiBEA zeolite were contacted with $Mn(NO_3)_2$ aqueous solution with appropriated concentration and stirred for 24 h at 298 K. Then, the suspensions were stirred in evaporator under vacuum of a water pump for 2 h at 333 K until the water was evaporated. The obtained materials were denoted as $Mn_{1.0}$SiBEA and $Mn_{2.0}$SiBEA where number next to element symbol refers to Mn wt % content. The as prepared Mn-containing SiBEA materials were calcined at 773 K (100 K h^{-1}) over 3 h and denoted as C-$Mn_{1.0}$SiBEA and C-$Mn_{2.0}$SiBEA.

2.2. Techniques

X-ray fluorescence chemical analysis was performed at room temperature on SPECTRO X-LabPro apparatus.

XRD experiments were done on a PANalytical Empyrean diffractometer equipped with the Cu Kα radiation (λ = 154.05 pm) in the 2θ range of 5°−90°.

Textural properties of studied samples were determined by low-temperature (77 K) N_2 sorption on an ASAP 2010 apparatus (Micromeretics). The zeolites, before analysis, were treated under vacuum at 623 K for 5 h. The specific surface area was calculated from the BET method. In order to determine the micropore volume the Dubinin-Radushkevich equation was used.

The OH groups environment and acidic properties of Mn-containing zeolites were determined by infrared spectroscopy as described in our previous work[18,19].

Diffuse reflectance UV−vis spectra were recorded in ambient atmosphere on a Cary 5000 Varian instrument with polytetrafluoroethylene as reference.

X-ray photoelectron spectroscopy (XPS) were carried out with Omicron (ESCA+) spectrometer, using an Al Kα (hν =1486.6 eV). X-ray source was equipped with a flood gun. The area of the analyzed sample was ca. 3 mm^2. The powder samples were prepared for measurements by pressed them on an indium foil. Binding energy (BE) of Mn, C, and O was calibrated to the Si 1s peak at 103.3 eV. Zeolite samples were outgassed at room temperature to a pressure of 10^{-7} Pa. All spectra were fitted with a Voigt function (a 70/30 composition of Gaussian and Lorentzian functions) in order to determine the number of components under each XPS peak.

EPR spectra were recorded on a JEOL FA-300 series EPR spectrometer at 9.3 GHz (X band) using a 100 kHz field modulation and a 5−10 G standard modulation width. The spectra were recorded at 298 and 77 K for fresh and calcined samples. The fresh $Mn_{2.0}$SiBEA sample was treated at 373, 473, 573 and 773 K for 2 h under a dynamic vacuum of 10^{-3} Pa at each temperature, which led to the activated Act-373-$Mn_{2.0}$SiBEA, Act-473-$Mn_{2.0}$SiBEA, Act-573-$Mn_{2.0}$SiBEA and Act-773-$Mn_{2.0}$SiBEA samples, respectively. Then Act-773-$Mn_{2.0}$SiBEA sample was reduced by treatment with pure H_2 at 543 K for 1 h what led to the Red-573-$Mn_{2.0}$SiBEA sample.

3. Results and discussion

3.1. XRD and FTIR Evidence for the Incorporation of Manganese into the Framework of SiBEA

The textural properties of zeolites before and after dealumination and after introduction of manganese ions were studied by means of low-temperature nitrogen sorption. **Figure 1** exhibits nitrogen sorption isotherms of TEABEA, HAlBEA, SiBEA, and

$Mn_{1.0}$SiBEA. All of them are type I according to IUPAC. The values of BET specific surface area and micropore volumes of HAlBEA, SiBEA, and $Mn_{1.0}$SiBEA were in the ranges of 613−669 m^2 g^{-1} and 0.25–0.27 cm^3 g^{-1}, respectively (**Table 1**). Those characteristics are typical of BEA zeolites.[20,21] The two-step postsynthesis procedure used for samples preparation did not significantly change the textural properties of zeolites upon acid treatment and the introduction of manganese into SiBEA support. Only TEABEA zeolite possessed low specific surface area and micropore volume due to presence of the organic TEA template in the structure of this zeolite, which might have blocked access to same pores. However, the acid treatment as well as the calcination led to removal of the organic compounds and increase of S_{BET} and V_{mic} values.

An analysis of zeolite BEA structure modifications may be done by XRD involving monitoring of the main reflection position at $2\theta = 22.3°–22.6°$, corresponding to d_{302} spacing, within a given series of zeolite samples. The d_{302} spacing for all studied samples were calculated from the corresponding 2θ value and summarized in **Table 2**. The d_{302} spacing decreased from 3.9788 Å for TEABEA to 3.9497 Å for HAlBEA and to 3.9206 Å for SiBEA indicating a matrix contraction, consistent with the removal of Al atoms from zeolite BEA structure. The introduction of Mn into SiBEA resulted in the increase of the d_{302} spacing from 3.9206 Å for SiBEA to 3.9365 Å for $Mn_{1.0}$SiBEA and to 3.9725 for C-$Mn_{1.0}$SiBEA (**Figure 2**). Those changes in the position of the main diffraction peak suggest expansion of the BEA structure and the incorporation of manganese ions into the vacant T–atom sites forming isolated, mononuclear Mn species in line with our earlier reports on VSiBEA[22] and MoSiBEA[23] zeolites. Furthermore, all diffractograms are typical of zeolite BEA phase with no proofs of the structure amorphization and appearance of other crystalline phases, suggesting that the removal of aluminum by nitric acid treatment did not damage zeolite structure.

The FT-IR spectra of HAlBEA, SiBEA and $Mn_{1.0}$SiBEA are showed in the **Figure 3**. The insightful analysis and descriptions of the FTIR results obtained on HAlBEA and SiBEA were done in our previous work.[17] It is well seen that the acid treatment of parent TEABEA zeolite led to removal of Al species and resulted in obtaining an aluminum free SiBEA with vacant T-atom sites (**Scheme 1**). The introduction of Mn into SiBEA zeolite led to the strong decrease in the intensity of the bands at 3520 and 3705 cm^{-1} related to OH groups forming hydroxyl nests indicating that a specific reaction between them and Mn ions took place. Moreover, the appearance of a new band at 3625 cm^{-1} was due to formation of Mn–O(H)–Si moieties (**Scheme 1, Structure C**), similar to acidic hydroxyl groups typical for zeolite materials. Thus, Mn ions were incorporated into vacant T-atom sites as isolated, framework species.

The FT-IR investigation associated with pyridine sorption may reveal not only the number of acidic sites but also their strength and different nature. The difference spectra of pyridine adsorbed on HAlBEA, SiBEA, $Mn_{1.0}$SiBEA and $Mn_{2.0}$SiBEA are shown in **Figure 4**. In the case of HAlBEA zeolite intensive bands of pyridinium cations and coordinately bonded pyridine molecules are seen. This indicates presence of Brønsted acidic sites as well as Lewis acidic sites in line with other works on aluminosilicate materials[19,24]. Pyridinium cations (bands at 1546 and 1638 cm^{-1}) and pyridine coordinately bonded to Lewis acidic sites (bands at 1622, 1491, and 1455 cm^{-1}) are present in the FT-IR spectra even after outgassing of HAlBEA at 573 K (**Table 2**), suggesting the strong acidic character of both Brønsted and Lewis acidic sites in this zeolite. In contrast, for SiBEA very low intense bands at 1638, 1546, and 1491 cm^{-1} are observed, indicating the presence of only a little amounts of Brønsted and Lewis acidic sites (**Figure 4 and Table 2**). The introduction of manganese in SiBEA resulted in arising of the band at 1450 cm^{-1} suggesting the formation of new Lewis acidic sites in $Mn_{1.0}$SiBEA and $Mn_{2.0}$SiBEA due to the presence of framework mononuclear Mn(II) species

(**Scheme 1, Structure B**). Furthermore, in the FTIR spectra of $Mn_{1.0}$SiBEA and $Mn_{2.0}$SiBEA the intensity of the bands at 1546 and 1638 cm^{-1} increased suggesting the formation of an additional amount of Brønsted acidic sites probably due to the creation of mononuclear Mn(III) species as shown in **Scheme 1**, **Structure C**. Similar observations were reported for FeSiBEA zeolites by Hnat et al.[25] Moreover, after samples evacuation at 573 K concentration of Lewis acidic centers decreased about 50 % and 30 % for $Mn_{1.0}$SiBEA and $Mn_{2.0}$SiBEA, respectively, suggesting high strength of acidic sites related to mononuclear Mn species.

3.2 Nature and Environment of Mn sites in MnSiBEA zeolites evidenced by DR UV-Vis and XPS.

The X-ray photoelectron spectroscopy and diffuse reflectance UV-Vis spectroscopy are very common use for determination of the oxidation state and the coordination of metal complexes in solid materials. However, in the case of manganese the possibility of occurring of Mn species with various oxidation states causes difficulties in interpretation of the experimental results. The literature data of XPS and DR UV-vis bands related to different oxidation state and type of Mn species in catalytic materials are summarized in **Table 4** to facilitate the discussion of our results.

DR UV-Vis spectra of as-prepared $Mn_{1.0}$SiBEA and $Mn_{2.0}$SiBEA exhibit two bands at 305 and 480 nm. The former one may be related to charge transfer transition between O^{2-} ligands and Mn(II) in the particular environment, in line with other reports on Mn-containing zeolites.[4,26,27] The band at 480 nm suggests presence of mononuclear Mn(III) probably as isolated species in pseudo-tetrahedral or octahedral coordination.[4,28,29] Thus, it seems that some part of initial Mn(II) was oxidize to Mn(III) during preparation procedure. After calcination intensity of bands at around 495 – 520 nm increased indicating larger contribution of Mn(III) in studied samples. Taking into account the positions of DR UV-Vis bands it may

be believed that in C-MnSiBEA zeolites manganese is mostly present as framework, mononuclear Mn(II) and Mn(III). Due to the lack of bands with maximum at 550 – 800 nm, the presence of Mn(IV) may be excluded.[28,30,31]

In the case of manganese compounds, the XPS spectroscopy allows determining the oxidation state of manganese. However, it is very difficult to determine the coordination state of this element in zeolites. **Figure 6** exhibits XPS spectrum of C-$Mn_{2.0}$SiBEA with peaks of Mn $2p_{3/2}$ range at 640.6 and 642.0 eV and of Mn $2p_{1/2}$ range at 652.7 and 654.1 eV. According to the literature data peaks at 640.6 and 652.7 eV are ascribed to Mn(II) species.[1,3] On the other hand, bands at 642.0 and 654.7 eV are typical for Mn(III) species in zeolites.[32,33] Moreover, signals typical for Mn(IV) are not seen at XPS spectrum of this zeolite[34,35] suggesting lack of Mn(IV) in studied sample. Thus, in C-$Mn_{2.0}$SiBEA manganese is predominantly present as framework, mononuclear Mn(II) and Mn(III). This statement is in an agreement with DR UV-Vis results.

3.3 EPR

The electron paramagnetic resonance spectroscopy is a powerful tool for the identification of paramagnetic transition metal species due to high sensitivity and unique spectrum shape related to nature and environment of the species occurring in a studied sample.

The X-band EPR spectrum of Mn(II) species in a disorder state consists of six major lines.[36] Generally, Mn(II) species in zeolites may be present as (i) framework mononuclear Mn(II), (ii) isolated Mn^{2+} ions in extra-framework positions, (iii) small clusters and (iv) oxides of MnO in extra-framework positions. Mn(II) species in framework positions, (ii) isolated Mn^{2+} ions in extra-framework positions, (iii) small clusters and (iv) oxides of MnO in extra-framework positions. According to Sinha et al.[37] first two types of Mn(II) species appear in EPR spectra as six major hyperfine lines, whereas the two later exhibits broad resonance

features. The contribution of certain Mn(II) species in zeolite samples depends on a preparation procedure and the manganese concentration. For the fresh samples, $Mn_{1.0}$SiBEA and $Mn_{2.0}$SiBEA, the broad EPR signal appears at room temperature (**Fig. 7**) and at 77 K (**Fig. 8**). On the other hand, hyperfine splitting can be resolved for samples after calcination (C-$Mn_{1.0}$SiBEA and C-$Mn_{2.0}$SiBEA). Moreover, for both calcined samples several additional lines can be observed in between the six main hyperfine lines for measurements at 77 K**.** These additional lines are assigned to $\Delta m_i = \pm 1$ forbidden transitions in line with previous reports on Mn(II) containing zeolites.[38,39]

Presence of broad EPR signal for fresh samples may be related to interactions of Mn(II) ions being in close vicinity to each other as well as presence of remaining precursor NO_3^- anions after impregnation step. This may also indicate that manganese ions were not completely incorporated into the SiBEA framework. However, calcination step led to removal of precursor anions and strong incorporation of manganese species into zeolite beta framework as mononuclear Mn(II). This is confirmed by well-resolved EPR signal for C-$Mn_{1.0}$SiBEA and C-$Mn_{2.0}$SiBEA typical for isolated, hydrated Mn(II) species.[11,28,40] Nevertheless, it is important to mention that authors of previous works on Mn-containing zeolite indicated that high quality EPR signal might be obtained only for samples with low Mn content. In our case, spectra for calcined samples are very well resolved even when they contained up to 2 wt % of Mn. This is additional evidence that in our samples manganese is present as well dispersed framework, mononuclear species.

An additional EPR experiment carried out for $Mn_{2.0}$SiBEA sample was performed in special reactor operated under vacuum and at different temperatures. The investigation revealed that with increasing temperature from room temperature up to 573 K (**Fig. 9**) decrease in EPR signal intensity was observed suggesting gradual oxidation of Mn(II) to Mn(III). However, when temperature was raised to 773 K a reverse increase in EPR signal

intensity took place indicating an auto-reduction of Mn(III) to Mn(II) due to the high temperature and the high vacuum. After that, the studied sample was treated in flowing hydrogen at 573 K. A sharp decrease in signal intensity was seen indicating that H_2-treatment caused reduction of large part of Mn(II) species to EPR silent Mn(I) and/or Mn(0) species. The same conclusions were drawn from EPR measurements carried out at 298 as at 77 K (**Fig. 10**).

Conclusions

The two-step postsynthesis method is an excellent way to obtain mononuclear manganese species in the framework of SiBEA zeolite without considerable changes in textural and structural properties of BEA zeolite.

The XPS, EPR, DR UV-Vis and FTIR investigations shown that manganese is incorporated into framework of BEA zeolite as isolated species and is present at two oxidation degree Mn(II) and Mn(III)

Framework manganese species create new type of Bronsted and Lewis acid sites in MnSiBEA zeolite.

EPR measurements performed on the zeolite samples after different treatment revealed that manganese species presence in $Mn_{1.0}$SiBEA and $Mn_{2.0}$SiBEA might easily change their oxidation state what will have important effect on the catalytic properties of these materials.

ACKNOWLEDGMENT

This project was funded by the National Science Center “PRELUDIUM” UMO-2012/07/N/ST5/00171 (R.B., S.D.).

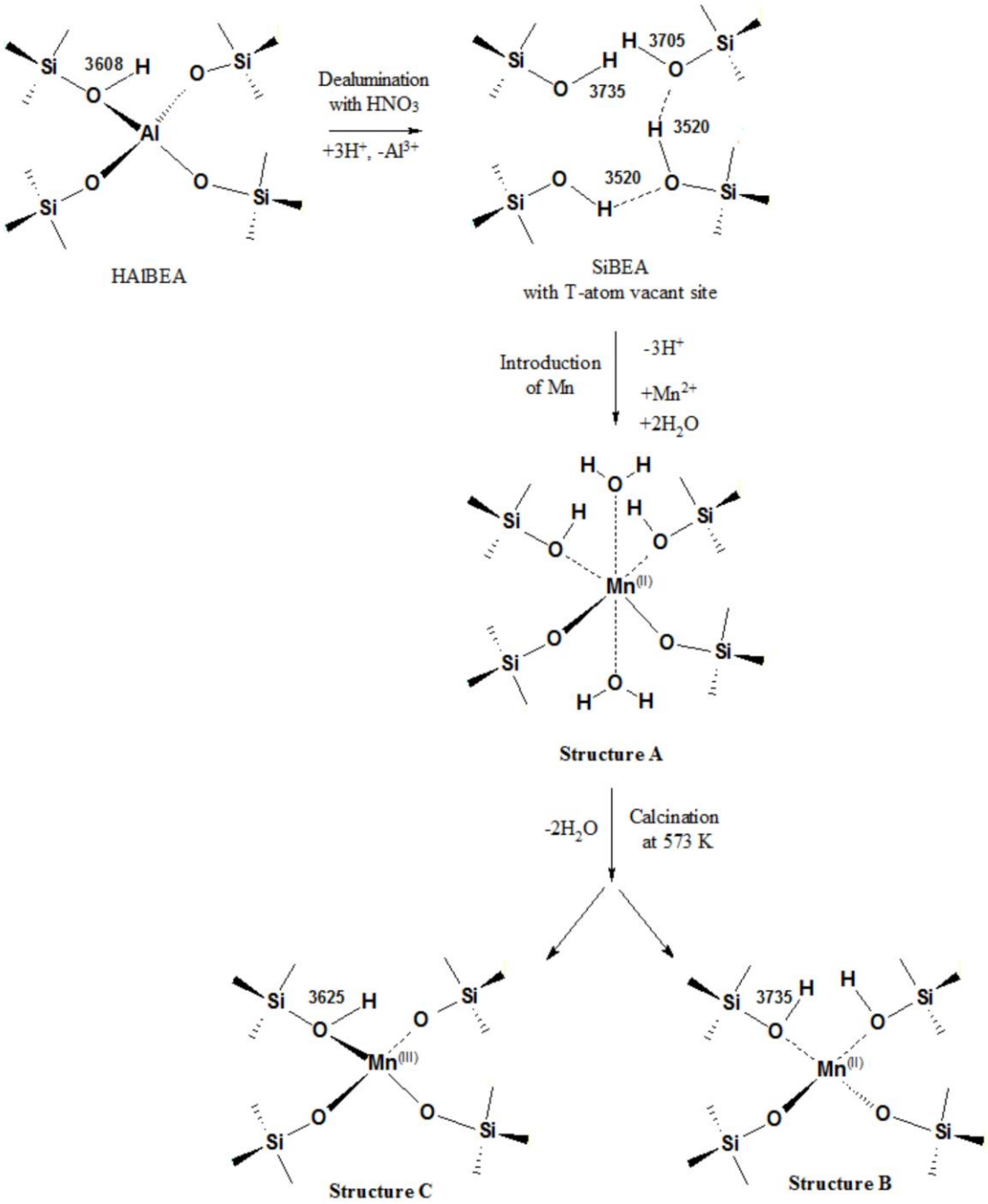

Scheme 1. Proposed way of formation of different states of Mn species in MnSiBEA zeolite.

Table 1. Textural properties of selected zeolite samples.

Sample	Specific surface area, S_{BET} ($m^2\ g^{-1}$)	Micropore volume, V_{mic} ($cm^3\ g^{-1}$)
TEABEA	58	0.03
HAlBEA	626	0.26
SiBEA	613	0.25
$Mn_{1.0}$SiBEA	669	0.27

Table 2. XRD parameters of selected zeolite samples.

Sample	2θ (◦)	d_{302} (Å)
TEABEA	22.326	3.9788
HAlBEA	22.493	3.9497
SiBEA	22.662	3.9206
$Mn_{1.0}$SiBEA	22.569	3.9365
C-$Mn_{1.0}$SiBEA	22.362	3.9725

Table 3. Amounts of Brønsted and Lewis acidic centers in HAlBEA, SiBEA, $Mn_{1.0}$SiBEA and $Mn_{2.0}$SiBEA.

Sample	Brønsted acidic centers (μmol g^{-1})		Lewis acidic centers (μmol g^{-1})	
	423 K	573 K	423 K	573 K
HAlBEA	333	247	137	128
SiBEA	8	3	3	1
$Mn_{1.0}$SiBEA	22	8	74	37
$Mn_{2.0}$SiBEA	26	6	136	93

Table 4. Literature data of DR UV-Vis and XPS bands of manganese in various oxidation states and environments.

Range of DR UV-Vis bands (nm)	Type of species	Compounds
250 – 325	Mn^{2+} ions framework Mn(II) framework Mn(III)	Mn-ZSM-5[4]
		Mn-BEA[26]
		Mn-Y[27]
390 – 500	extra-framework Mn(II) and Mn(III)	MnMCM-41[28]
		Mn-ZSM-5[4]
		Mn-APO-31[29]
500 – 800	extra-framework Mn(III) and Mn(IV) (oxides clusters)	CeO_2– MnO/SiO_2[30]
		Mn-SBA-15[31]
		Zn/Mn-MCM-41[28]
Range of XPS bands (eV)	Oxidation state	Compounds
640 – 641	Mn(II)	10%Mn/USY[1]
		1.6MnCBV[3]
641 – 642	Mn(III)	Ag-Mn/H-BEA[32]
		Mn/Ce–ZrO_x[33]
643 – 644	Mn(IV)	Mn/ZSM-5[34]
		AgMn/HZSM-5[35]

Figure captions

Figure 1. Adsorption isotherms of nitrogen at 77 K of TEABEA, SiBEA, HAlBEA and $Mn_{1.0}$SiBEA samples. Full symbols: adsorption; empty symbols: desorption. For convenience, the dataset for SiBEA, HAlBEA and $Mn_{1.0}$SiBEA were shifted upwards along the Y-axis.

Figure 2. XRD patterns recorded at room temperature of TEABEA, HAlBEA, SiBEA, $Mn_{1.0}$SiBEA and C-$Mn_{1.0}$SiBEA.

Figure 3. FTIR spectra recorded at room temperature of HAlBEA, SiBEA and $Mn_{1.0}$SiBEA in the vibrational range of OH groups.

Figure 4. FTIR spectra recorded at room temperature of HAlBEA, SiBEA, $Mn_{1.0}$SiBEA and $Mn_{2.0}$SiBEA after adsorption of pyridine (133 Pa) for 1 h at room temperature and desorption at 423 K for 1 hour

Figure 5. DR UV-Vis spectra recorded at ambient atmosphere of $Mn_{1.0}$SiBEA, $Mn_{2.0}$SIBEA, C-$Mn_{1.0}$SiBEA and C-$Mn_{2.0}$SiBEA.

Figure 6. Mn 2p XP spectrum recorded at room temperature of C-$Mn_{2.0}$SiBEA.

Figure 7. EPR spectra recorded at room temperature of $Mn_{1.0}$SiBEA, $Mn_{2.0}$SiBEA, C-$Mn_{1.0}$SiBEA and C-$Mn_{2.0}$SiBEA.

Figure 8. EPR spectra recorded at 77 K of $Mn_{1.0}$SiBEA, $Mn_{2.0}$SiBEA, C-$Mn_{1.0}$SiBEA and C-$Mn_{2.0}$SiBEA.

Figure 9. EPR spectra recorded at 289 K of $Mn_{2.0}$SiBEA, Act-100-$Mn_{2.0}$SiBEA, Act-200-$Mn_{2.0}$SiBEA, Act-300-$Mn_{2.0}$SiBEA, Act-500-$Mn_{2.0}$SiBEA and Red-300-$Mn_{2.0}$SiBEA where Act states for activated (outgassed for 2 h under vacuum), Red states for reduced (treated with pure hydrogen for 1 h) and number prior to zeolite symbol states for treatment temperature.

Figure 10. EPR spectra recorded at 77 K of $Mn_{2.0}$SiBEA, Act-100-$Mn_{2.0}$SiBEA, Act-200-$Mn_{2.0}$SiBEA, Act-300-$Mn_{2.0}$SiBEA, Act-500-$Mn_{2.0}$SiBEA and Red-300-$Mn_{2.0}$SiBEA where Act states for activated (outgassed for 2 h under vacuum), Red states for reduced (treated with pure hydrogen for 1 h) and number prior to zeolite symbol states for treatment temperature.

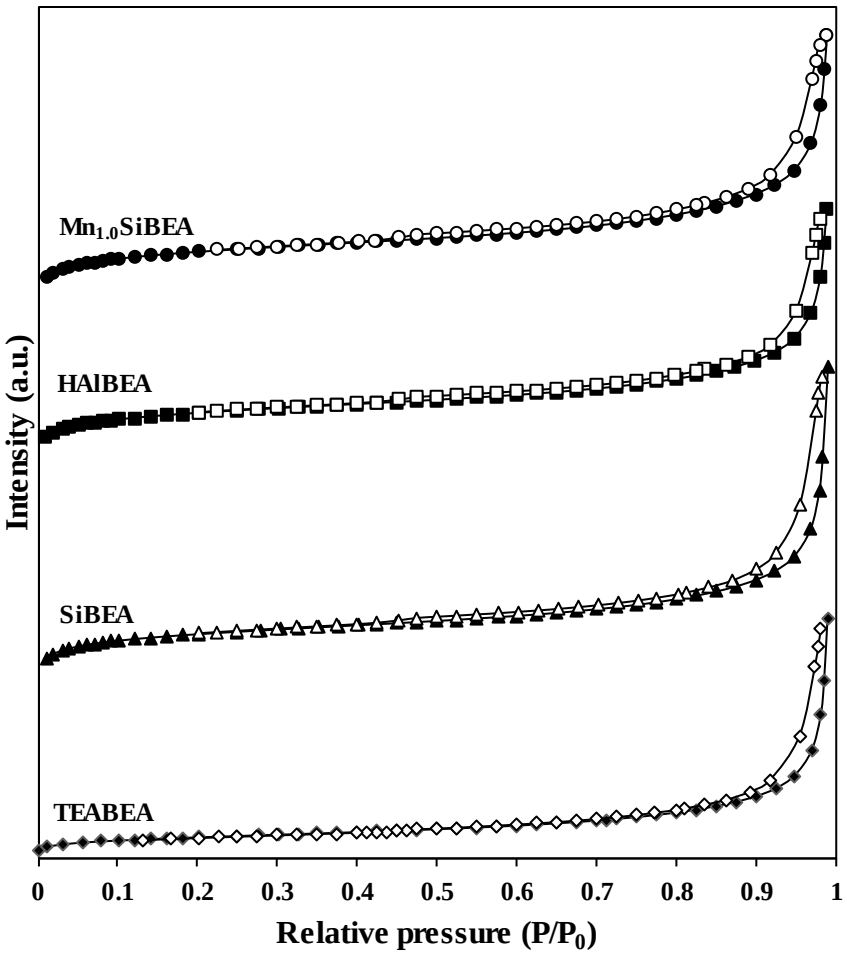
Mn1.0SiBEA
HAlBEA
SiBEA
TEABEA
Intensity (a.u.)
0
0.1
0.2
0.3
0.4
0.5
0.6
0.7
0.8
0.9
1
Relative pressure (P/P0)

Figure 1.

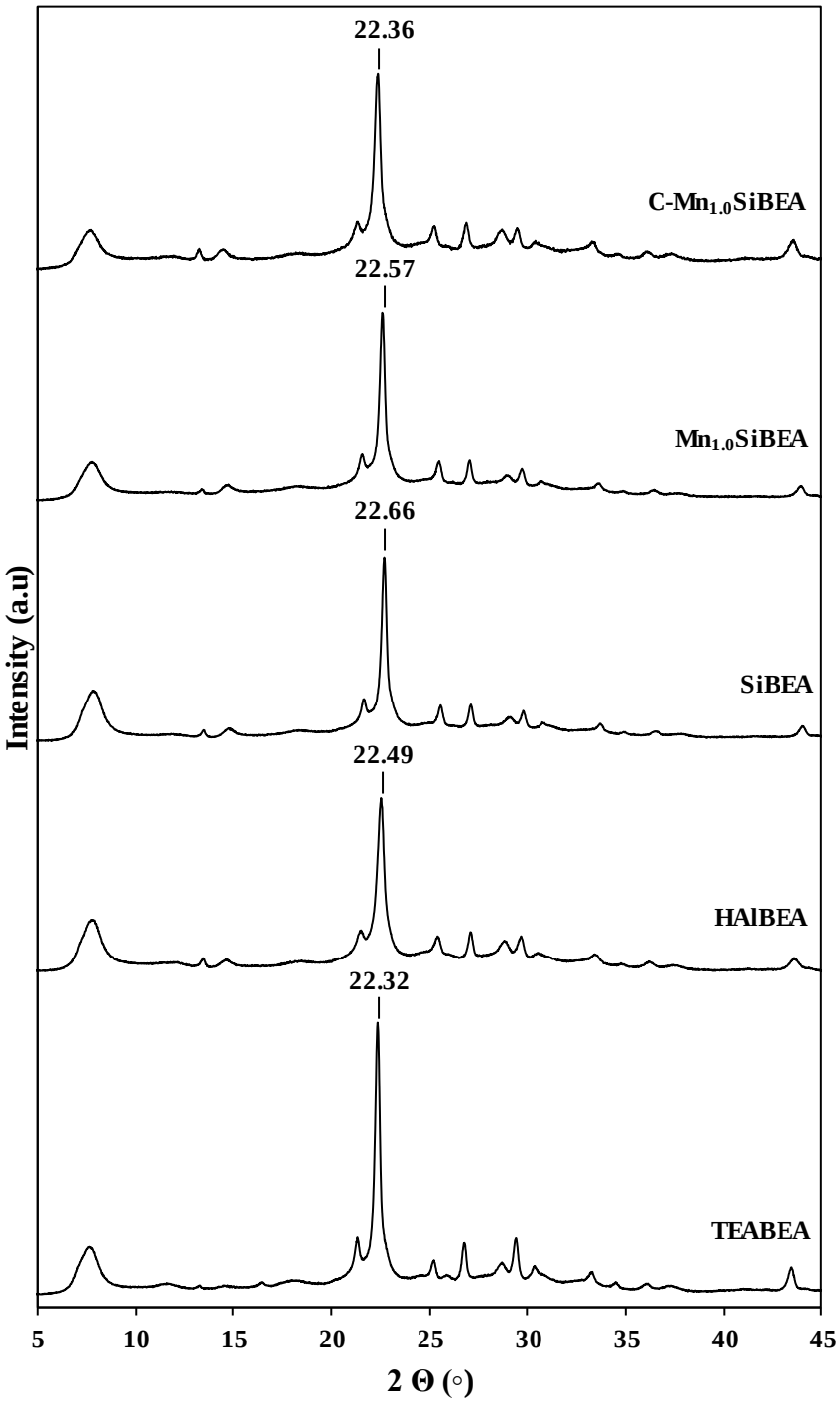
22.36
C-Mn1.0SiBEA
22.57
Mn1.0SiBEA
22.66
SiBEA
22.49
HAlBEA
22.32
TEABEA
Intensity (a.u)
5
10
15
20
25
30
35
40
45
2 Θ (◦)

Figure 2.

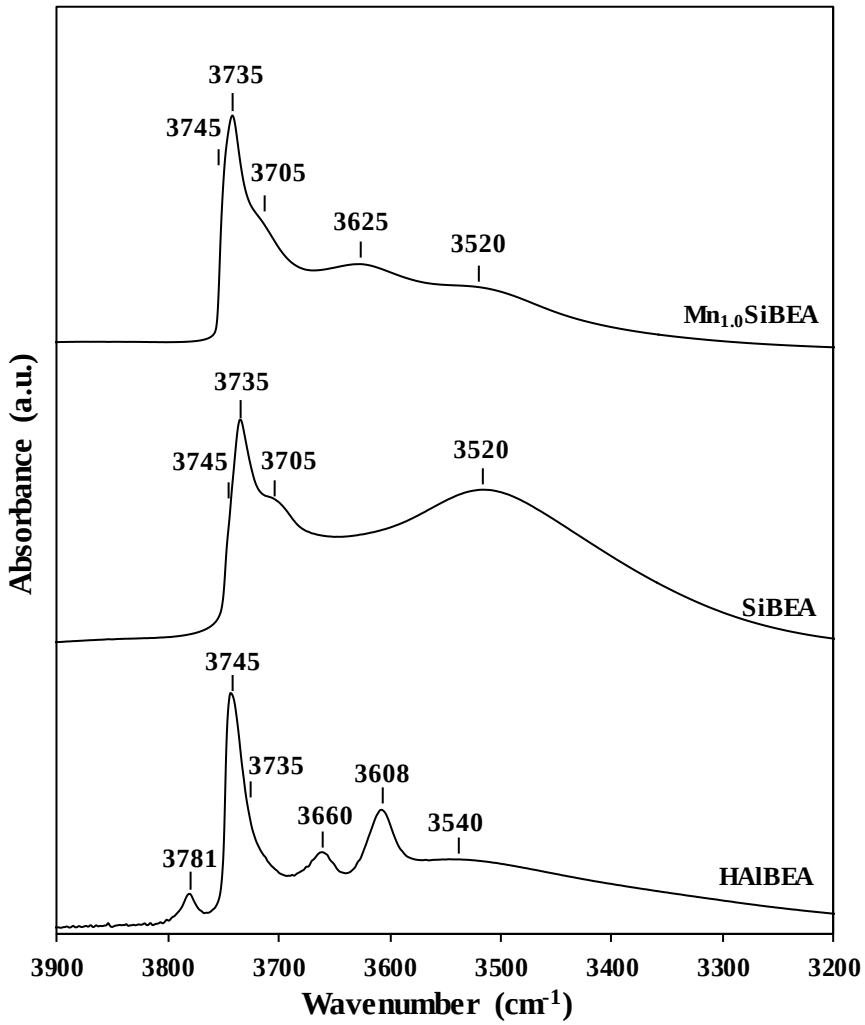
3735
3745
3705
3625
3520
Mn1.0SiBEA
3735
3745
3705
3520
SiBEA
3745
3735
3608
3660
3540
3781
HAlBEA
Absorbance (a.u.)
3900
3800
3700
3600
3500
3400
3300
3200
Wavenumber (cm-1)

Figure 3.

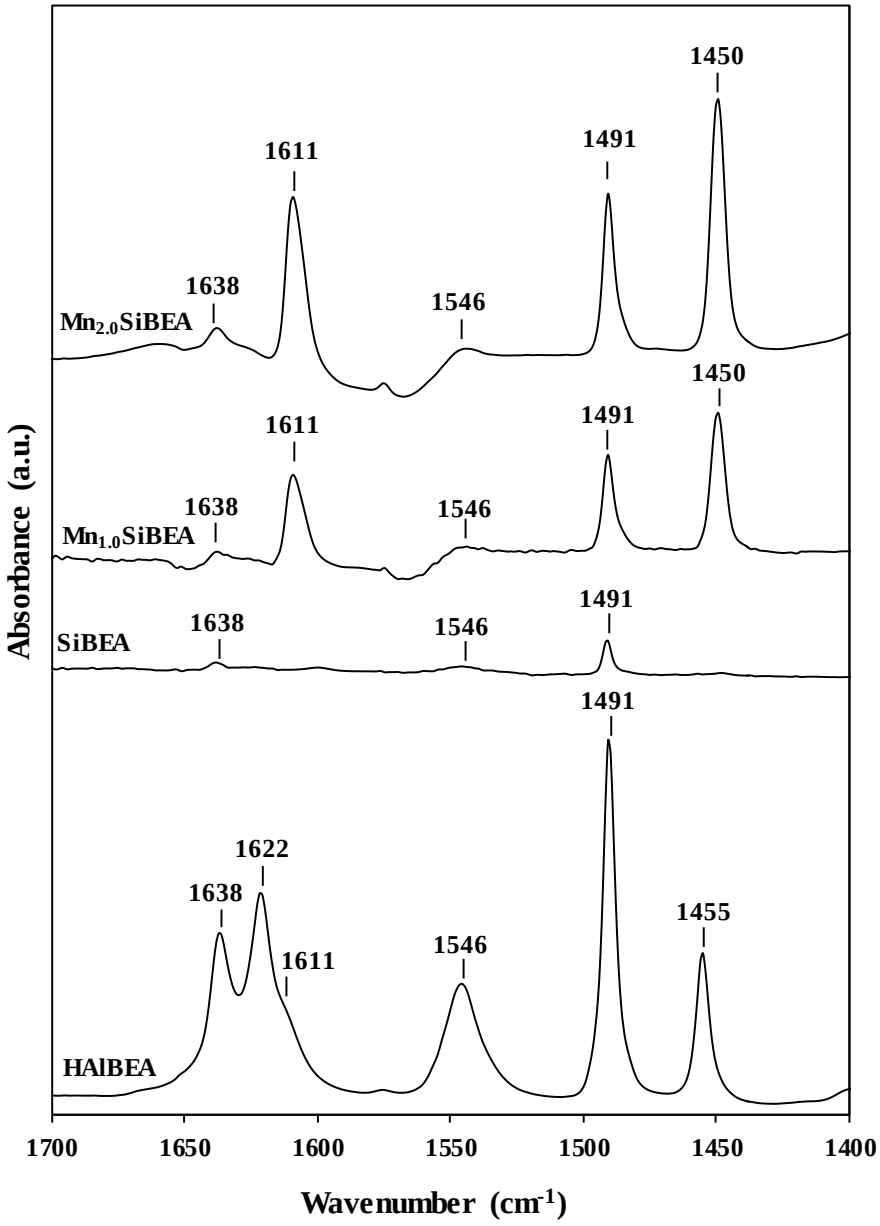
1450
1611
1491
1638
1546
Mn2.0SiBEA
1450
1611
1491
1638
1546
Mn1.0SiBEA
1491
1638
1546
SiBEA
1491
1622
1638
1455
1611
1546
HAlBEA
Absorbance (a.u.)
1700
1650
1600
1550
1500
1450
1400
Wavenumber (cm-1)

Figure 4.

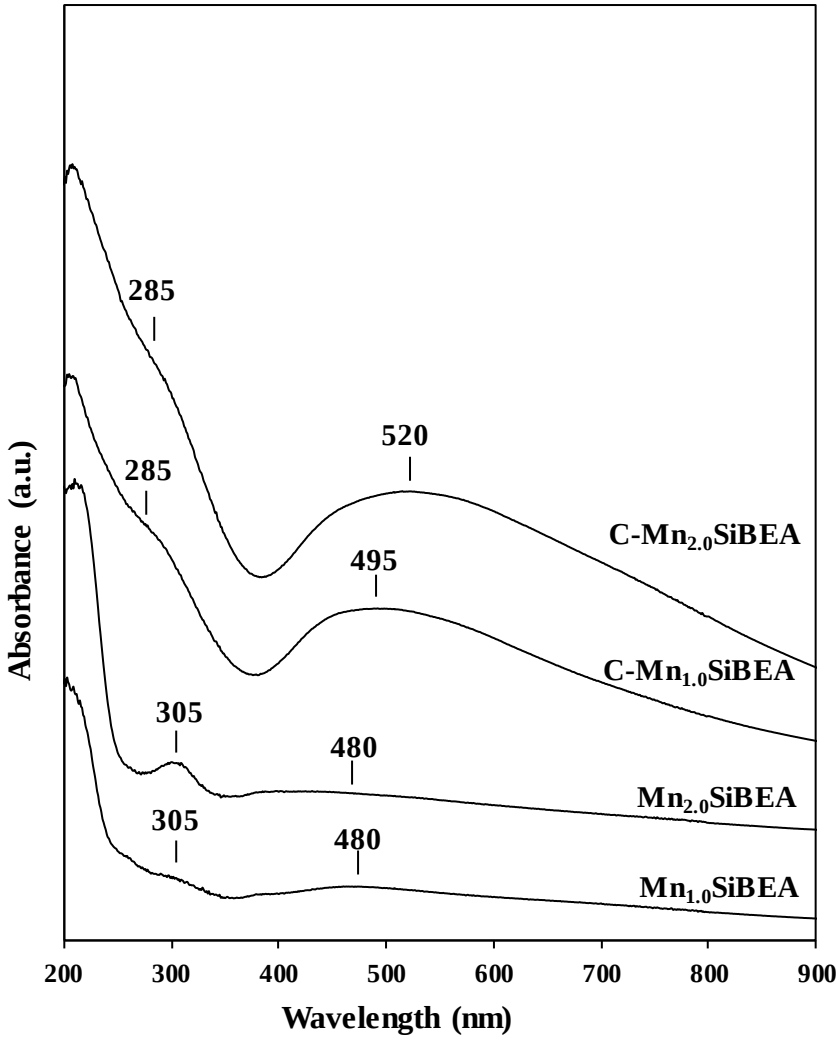
285
520
285
C-Mn2.0SiBEA
495
C-Mn1.0SiBEA
305
480
Mn2.0SiBEA
305
480
Mn1.0SiBEA
Absorbance (a.u.)
200
300
400
500
600
700
800
900
Wavelength (nm)

Figure 5.

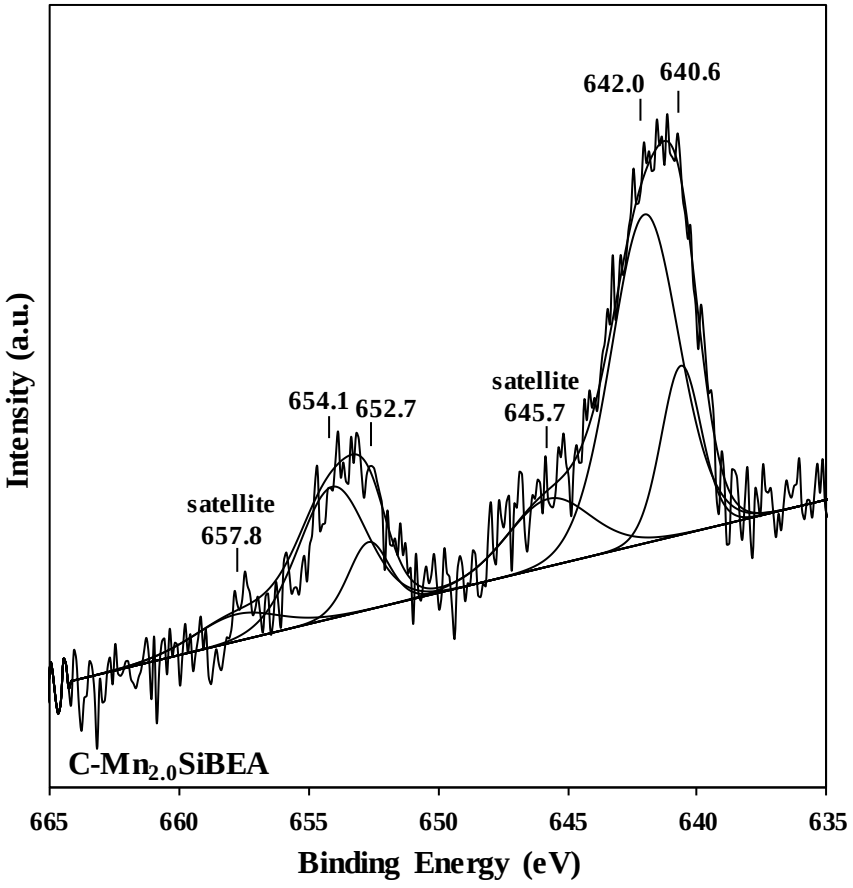
642.0
640.6
654.1
652.7
satellite
645.7
satellite
657.8
C-Mn2.0SiBEA
Intensity (a.u.)
665
660
655
650
645
640
635
Binding Energy (eV)

Figure 6.

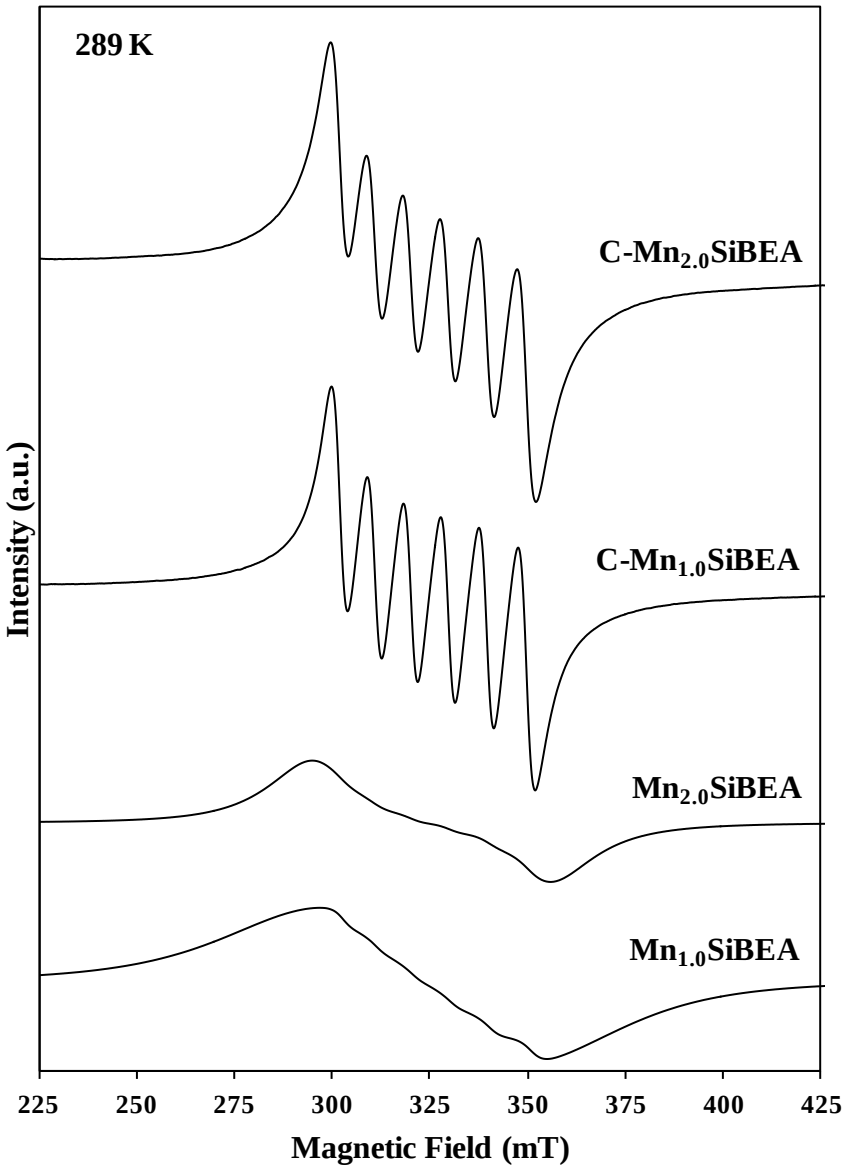
289 K
C-Mn2.0SiBEA
C-Mn1.0SiBEA
Mn2.0SiBEA
Mn1.0SiBEA
Intensity (a.u.)
225
250
275
300
325
350
375
400
425
Magnetic Field (mT)

Figure 7.

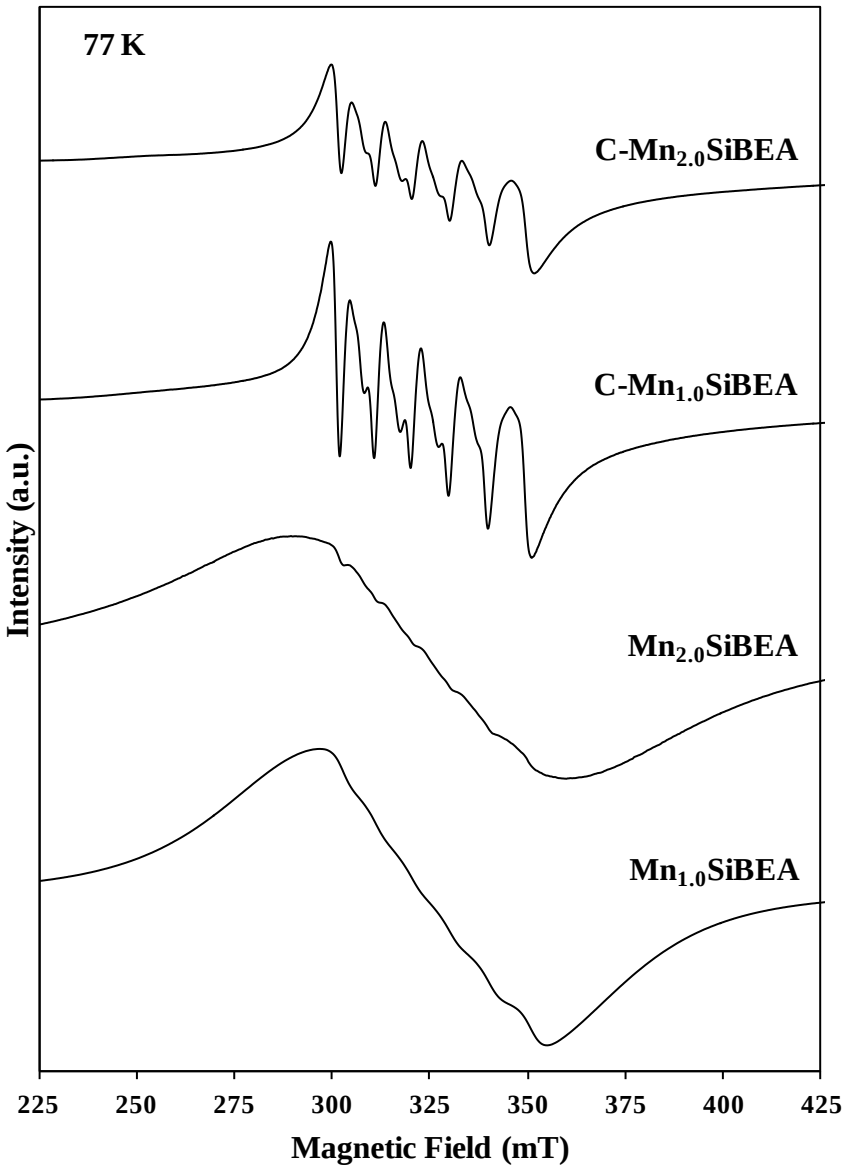
77 K
C-Mn2.0SiBEA
C-Mn1.0SiBEA
Mn2.0SiBEA
Mn1.0SiBEA
Intensity (a.u.)
225
250
275
300
325
350
375
400
425
Magnetic Field (mT)

Figure 8.

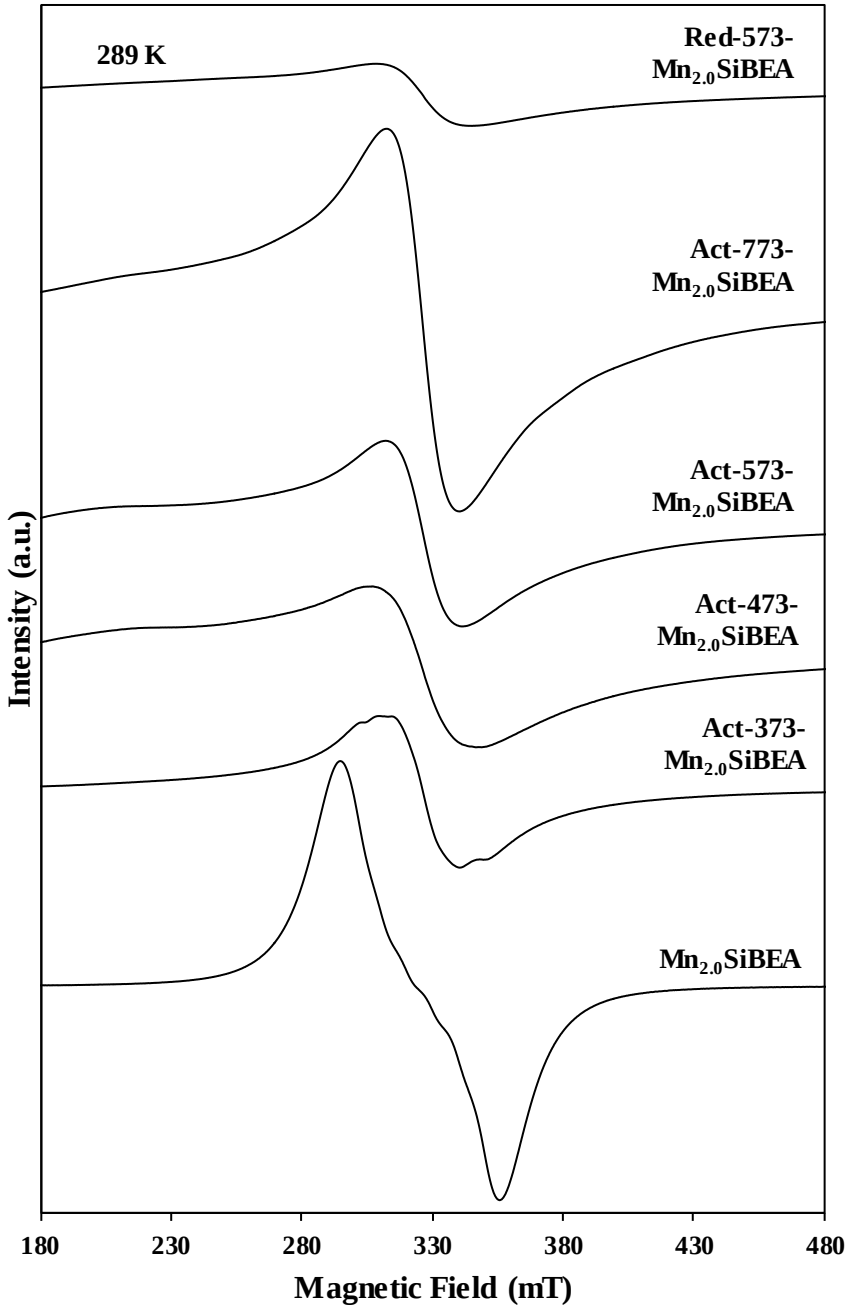
289 K
Red-573-Mn2.0SiBEA
Act-773-Mn2.0SiBEA
Act-573-Mn2.0SiBEA
Act-473-Mn2.0SiBEA
Act-373-Mn2.0SiBEA
Mn2.0SiBEA
Intensity (a.u.)
180
230
280
330
380
430
480
Magnetic Field (mT)

Figure 9.

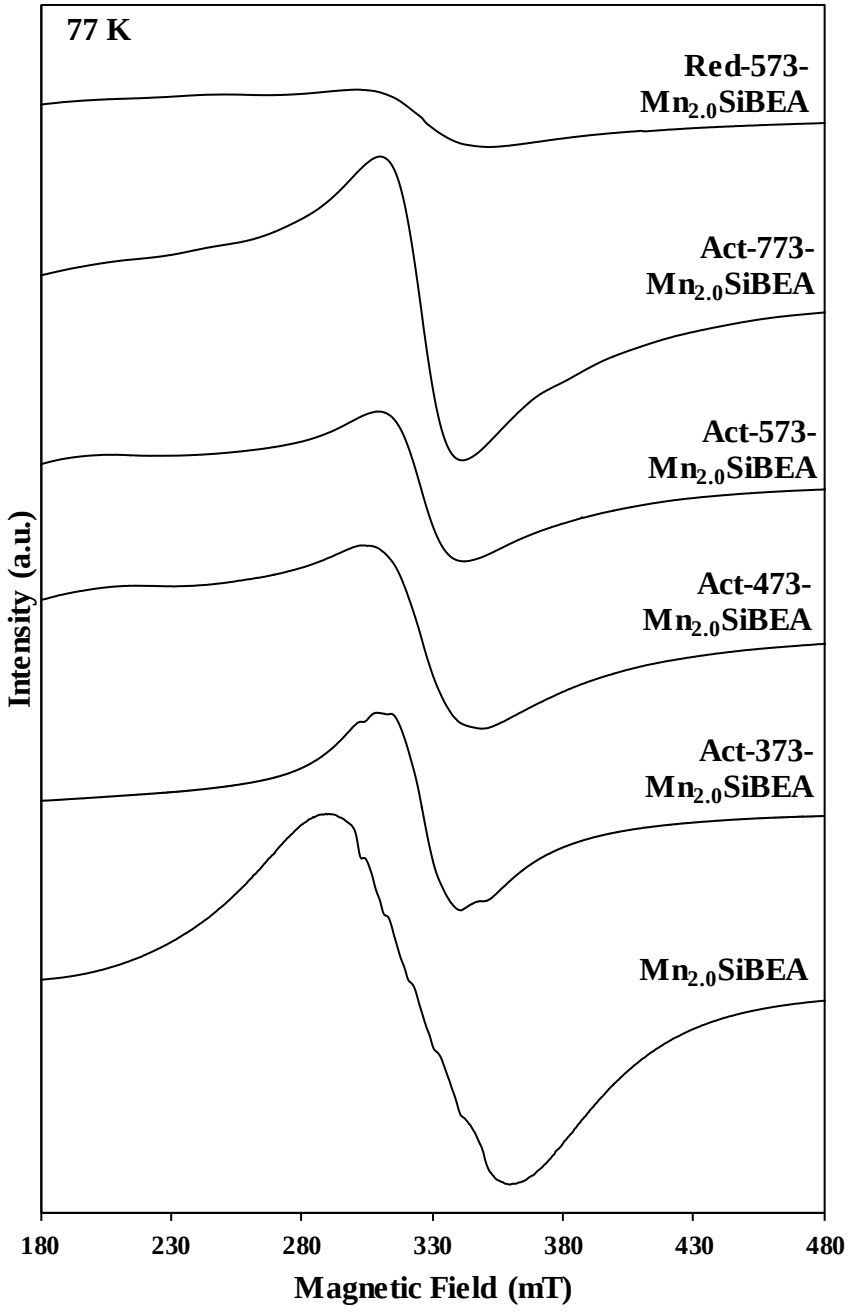
77 K
Red-573-Mn2.0SiBEA
Act-773-Mn2.0SiBEA
Act-573-Mn2.0SiBEA
Act-473-Mn2.0SiBEA
Act-373-Mn2.0SiBEA
Mn2.0SiBEA
Intensity (a.u.)
180
230
280
330
380
430
480
Magnetic Field (mT)

Figure 10.

References

1 Q. Lin, J. Li, L. Ma and J. Hao, *Catal. Today*, 2010, **151**, 251–256.

2 A. Sultana, M. Sasaki and H. Hamada, *Catal. Today*, 2012, **185**, 284–289.

3 M. Stanciulescu, G. Caravaggio, A. Dobri, J. Moir, R. Burich, J.-P. Charland and P. Bulsink, *Appl. Catal. B Environ.*, 2012, **123-124**, 229–240.

4 Y. Meng, H. C. Genuino, C. Kuo, H. Huang, S. Chen, L. Zhang, A. Rossi and S. L. Suib, *J. Am. Chem. Soc.*, 2013, **135**, 8594–8605.

5 H. Einaga and S. Futamura, *Catal. Commun.*, 2007, **8**, 557–560.

6 B. Z. Zhan, B. Modén, J. Dakka, J. G. Santiesteban and E. Iglesia, *J. Catal.*, 2007, **245**, 316–325.

7 H. Chen, M. Matsuoka, J. Zhang and M. Anpo, *J. Phys. Chem. B*, 2006, **110**, 4263–4269.

8 G. H. Jeong, Y. Kim and K. Seff, *Microporous Mesoporous Mater.*, 2006, **93**, 12–22.

9 S. N. Azizi and S. Ehsani Tilami, *J. Solid State Chem.*, 2013, **198**, 138–142.

10 N. Z. Logar, N. N. Tušar, G. Mali, M. Mazaj, I. Arčon, D. Arčon, A. Rečnik, A. Ristić and V. Kaučič, *Microporous Mesoporous Mater.*, 2006, **96**, 386–395.

11 M. Selvaraj, P. K. Sinha, K. Lee, I. Ahn, A. Pandurangan and T. G. Lee, *Microporous Mesoporous Mater.*, 2005, **78**, 139–149.

12 S. Dzwigaj, M. J. Peltre, P. Massiani, A. Davidson, M. Che, T. Sen and S. Sivasanker, *Chem. Commun.*, 1998, 87–88.

13 S. Dzwigaj, M. Matsuoka, R. Franck, M. Anpo and M. Che, *J. Phys. Chem. B*, 1998, **102**, 6309–6312.

14 S. Dzwigaj, P. Massiani, A. Davidson and M. Che, *J. Mol. Catal. A Chem.*, 2000, **155**, 169–182.

15 S. Dzwigaj, *Curr. Opin. Solid State Mater. Sci.*, 2003, **7**, 461–470.

16 S. Dzwigaj, E. Ivanova, R. Kefirov, K. Hadjiivanov, F. Averseng, J. M. Krafft and M. Che, *Catal. Today*, 2009, **142**, 185–191.

17 R. Baran, Y. Millot, T. Onfroy, J. M. Krafft and S. Dzwigaj, *Microporous Mesoporous Mater.*, 2012, **163**, 122–130.

18 R. Baran, T. Onfroy, S. Casale and S. Dzwigaj, *J. Phys. Chem. C*, 2014, **118**, 20445–20451.

19 A. Śrebowata, R. Baran, D. Łomot, D. Lisovytskiy, T. Onfroy and S. Dzwigaj, *Appl. Catal. B Environ.*, 2014, **147**, 208–220.

20 J. Zhu, Y. Zhu, L. Zhu, M. Rigutto, A. Van Der Made, C. Yang, S. Pan, L. Wang, L. Zhu, Y. Jin, Q. Sun, Q. Wu, X. Meng, D. Zhang, Y. Han, J. Li, Y. Chu, A. Zheng, S. Qiu, X. Zheng and F. S. Xiao, *J. Am. Chem. Soc.*, 2014, **136**, 2503–2510.

21 S. M. Maier, A. Jentys and J. a. Lercher, *J. Phys. Chem. C*, 2011, **115**, 8005–8013.

22 R. Baran, Y. Millot, T. Onfroy, F. Averseng, J.-M. Krafft and S. Dzwigaj, *Microporous Mesoporous Mater.*, 2012, **161**, 179–186.

23 R. Baran, F. Averseng, Y. Millot, T. Onfroy, S. Casale and S. Dzwigaj, *J. Phys. Chem. C*, 2014, **118**, 4143–4150.

24 R. Dębek, M. F. G. Ribeiro, A. Fernandes and M. Motak, *Comptes Rendus Chim.*, 2015, **18**, 1211–1222.

25 I. Hnat, I. Kocemba, J. Rynkowski, T. Onfroy and S. Dzwigaj, *Catal. Today*, 2011, **176**, 229–233.

26 Z. He, J. Wu, B. Gao and H. He, *ACS Appl. Mater. Interfaces*, 2015, **7**, 2424–2432.

27 B. Qi, X. H. Lu, D. Zhou, Q. H. Xia, Z. R. Tang, S. Y. Fang, T. Pang and Y. L. Dong, *J. Mol. Catal. A Chem.*, 2010, **322**, 73–79.

28 B. J. Aronson, C. F. Blanford and A. Stein, *J. Phys. Chem. B*, 2000, **104**, 449–459.

29 N. Novak Tusar, G. Mali, I. Arcon, V. Kaučič, A. Ghanbari-Siahkali and J. Dwyer, *Microporous Mesoporous Mater.*, 2002, **55**, 203–216.

30 T. Kharlamova, G. Mamontov, M. Salaev, V. Zaikovskii, G. Popova, V. Sobolev, A. Knyazev and O. Vodyankina, *Appl. Catal. A Gen.*, 2013, **467**, 519–529.

31 V. Mahdavi and M. Mardani, *Mater. Chem. Phys.*, 2015, **155**, 136–146.

32 H. Pan, Q. Su, J. Chen, Q. Ye, Y. Liu and Y. Shi, *Environ. Sci. Technol.*, 2009, **43**, 9348–53.

33 X. Zhang, B. Shen, K. Wang and J. Chen, *J. Ind. Eng. Chem.*, 2013, **19**, 1272–1279.

34 G. Lv, F. Bin, C. Song, K. Wang and J. Song, *Fuel*, 2013, **107**, 217–224.

35 Y. Liu, X. Li, C. Shi, J. Liu and A. Zhu, *Catal. Sci. Technol.*, 2014, **4**, 2589–2598.

36 S. Ashtekar, A. M. Prakash, D. K. Chakrabarty and S. V. V Chilukuri, *J. Chem. Soc. Faraday Trans.*, 1996, **92**, 2481–2486.

37 A. K. Sinha, C. V. V Satyanarayana, D. Srinivas, S. Sivasanker and P. Ratnasamy, *Microporous Mesoporous Mater.*, 2000, **35-36**, 471–481.

38 G. Brouet, X. Chen, C. Lee and L. Kevan, *J. Am. Chem. Soc.*, 1992, **114**, 3720–3726.

39 Z. Olender, D. Goldfarb and J. Batista, *J. Am. Chem. Soc.*, 1993, **115**, 1106–1114.

40 S. Gomez, O. Giraldo, L. J. Garces, J. Villegas and S. L. Suib, *Chem. Mater.*, 2004, **16**, 2411–2417.